Human β-defensin 4 – defensin without the "twist"

ABSTRACT

β-defensins are small, cysteine-rich, cationic peptides that contribute to various processes related to both arms of host defense, the innate and adaptive immunities. All β-defensins are potent antimicrobials with activity targeting a broad range of pathogens. Some human β-defensins (hBDs) are also capable of binding and activating specific chemokine receptors, leading to chemotaxis of receptor-presenting cells. Two receptors identified as targets of specific human β-defensins are CCR2 and CCR6, both members of the seven-transmembrane family of chemokine receptors. Currently, around 50 open reading frames (ORFs) identified in the human genome encode proteins that have signatures characteristic of β-defensins. Of those, only three, hBD1-3, have been thoroughly characterized to date, including a detailed structural description of their molecules. In addition, limited information on biological and bactericidal properties is available for hBD4, as well as the solution structure of hBD6. The crystal structure of hBD4, determined here at resolution of 1.60 Å, indicates significant structural differences between this molecule and those reported previously for other hBDs. Crystallographic studies indicate a possibility of unique dimerization of hBD4, confirmed by solution studies using analytical ultracentrifugation. In contrast to hBD1-3, hBD4 does not induce CCR6-mediated chemotaxis. This observation can be attributed to an unusual conformation of the hBD4 N-terminus. In agreement with previously published reports, hBD4 was shown to be a potent antibacterial agent, as demonstrated by results of assays with *E. coli* ATCC 25922 cells.

INTRODUCTION

Defensins are a group of small, β-sheet-rich, cationic and amphipathic proteins whose molecules adopt a conserved structural fold, usually stabilized by six invariant cysteine residues [1,2]. These peptides were identified in many multicellular organisms, including plants [3], invertebrate [4] and vertebrate animals [5], as well as in insects [6]. Around 50 ORFs with sequences bearing signatures of defensins have been identified in the human genome [7]. Human defensins are organized into two classes, α- and β-defensin, based primarily on the spacing between the cysteine residues and the topology of disulfide bridges [2]. Whereas the six cysteine residues in α-defensins form disulfide bonds with the topology Cys^1-Cys^6, Cys^2-Cys^4, and Cys^3-Cys^5 (or 1-6, 2-4, 3-5), the connectivity in native forms of β-defensins has the topology 1-5, 2-4, 3-6.

All β-defensins characterized to date have a capacity to kill or inhibit *in vitro* a wide variety of bacteria and fungi, particularly at low concentrations of salt and plasma proteins [2,8,9]. In addition to the antimicrobial properties of β-defensins, these proteins were also shown to be potent immunomodulators, suggesting their important role in regulating both innate and adaptive immunities [10, 11]. Some of these activities are associated with chemotactic properties of β-defensins due to their ability to interact with specific chemokine receptors [11-13]. It was shown that hBD1-3 bind to the chemokine receptor CCR6 expressed on immature dendritic cells and CD45RO+ and CD4+ T cells [12], whereas activation of another receptor, CCR2, by human β-defensins 2 and 3 triggers chemotaxis of monocytes, macrophages, and neutrophils [14]. Interaction with CCR2 was also reported for human β-defensin 6 [15,16].

The molecular bases of antimicrobial activity of defensins have been researched extensively [17-19]. These studies resulted in some understanding of the structural determinants of this activity and led to a few models (hypotheses) describing interactions between defensins and bacteria [20-23]. It is possible, however, that no single model satisfactorily describes the mechanism of antimicrobial properties of even a small group of related defensins, and that activity is a result of several processes, each controlled by a different mechanism [24].

Molecular features of β-defensins associated with their chemotactic properties are still poorly understood. The first attempt to identify structural features of

Adam Prahl[1]

Marzena Pazgier[2]

Jerry Alexandratos[3]

Jacek Lubkowski[3, ✉]

[1]Faculty of Chemistry, Department of Organic Chemistry, University of Gdansk, Gdansk, Poland
[2]Division of Vaccine Research, Institute of Human Virology, University of Maryland School of Medicine, Baltimore, MD, USA
[3]Macromolecular Crystallography Laboratory, Center for Cancer Research, National Cancer Institute, Frederick MD, USA

✉NCI-Frederick, 539, Frederick, MD 21702, USA; phone: (301) 846 54 94, fax: (301) 846 71 01, e-mail: lubkowsj@mail.nih.gov

Table 1. Details of the production and crystallization of recombinant hBD4.

Cloning and Expression	
Source organism	*Homo sapiens*
DNA source	Synthetic
Expression vector	pAED4
Expression host	*E. coli* BL21(DE3)pLysS
Complete amino acid sequence of the construct produced	EFELDRICGY GTARCRKKCR SQEYRIGRCP NTYACCLRKW DESLLNRTKP
Crystallization	
Method	Hanging-drop vapor diffusion
Plate type	Linbro 24 well
Temperature (K)	293
Protein concentration (mg·ml-1)	28
Buffer composition of protein solution	50 mM Tris-HCl pH 7.5, 150 mM NaCl
Composition of reservoir solution	25.5% PEG 8,000, 0.085 M sodium acetate buffer pH 4.5, 0.17 M Lithium Sulfate, 15% Glycerol
Composition of droplet	1μl (protein) + 1 μl (reservoir)
Volume of reservoir (ml)	1.0

β-defensins, relevant for interaction with CCR6, was based on a comparison of hBD1 and hBD2 structures with the structure of the native ligand of this receptor, the macrophage inflammatory protein 3α (MIP-3α) [25,26]. These reports suggested the N-terminal α-helix and a few other residues distributed on surfaces of β-defensins as important for activation of CCR6. Similar motifs have been also implied recently for this β-defensin based on NMR experiments mapping interactions between hBD6 and extracellular fragments of CCR2 [15,16]. Subsequently, the significance of the N-terminal section of hBD1-3 molecules for interactions with CCR6 was observed during structural and functional studies of hBD1 mutants [27]. The importance of the N-terminal region was also demonstrated for Defb14, a mouse orthologue of hBD3 [28]. Correlations between the topology of three disulfide bonds and chemotactic properties of human β-defensin 3 were reported in studies of engineered variants of hBD3 [23]. Taylor and coworkers reported the fifth canonical Cys residue as critical for CCR6-mediated chemotactic properties of hBD3 [29]. Currently, the knowledge of structural properties of human β-defensins is still quite sparse, and limited to four members of this class hBD1 [30], hBD2[31], hBD3 [32], and hBD6 [15] as well as a series of their mutated forms.

Human β-defensin 4 was originally identified by *in silico* screening of genomic sequences [33]. The same authors showed that synthetic hBD4 has strong bactericidal properties, in particular against *Pseudomonas aeruginosa,* and that it is chemotactic for human blood monocytes. They also identified hBD4 mRNA expression in testis, stomach, uterus, neutrophils, thyroid, lung, and kidney. Information on tissue distribution of hBD4 under disease conditions or pathogen exposure as well as on antibacterial properties of this defensin was presented in several subsequent reports [34-37]. Low copy number of hBD4-encoding gene, DEFB4, was associated with susceptibility to cervical cancer [38]. Sharma and coworkers studied the role of disulfide bonds on antibacterial properties of hBD4 [39,40]. In comparison to thousands of publications describing properties and biological roles of the first three human β-defensins(1-3), hBD4 is only minimally characterized. The current body of literature referring to this defensin is limited to just a few tens of publications. In particular, a structural description of the hBD4 molecule is missing, making impossible a direct comparison with hBD1-3 or a possible correlation between structural and functional properties. In an attempt to fill this niche, we present in this report results of structural, biophysical and functional studies of a recombinant hBD4.

MATERIALS AND METHODS

CLONING, EXPRESSION, FOLDING AND PURIFICATION OF RECOMBINANT hBD4

The cDNA sequence encoding mature hBD4 was obtained from GenBank (Ref. No, BC100849.1; see also Tab. 1). The DNA sequence was codon-optimized for expression in *E. coli* using the program DNAWorks [41]. Gene assembly and amplification were performed as previously described [41] The purified product of the PCR assembly, containing the synthetic hBD4 coding sequence preceded by the Met and Trp codons and flanked with *Hind*III and *Bam*HI restriction sites, was integrated into the pAED4 vector (Addgene) that encoded a fragment of the *E. coli* tryptophan operon (trp ΔLE 1413 polypeptide) [42]. Additionally, the (His)$_6$ affinity-tag coding sequence was inserted directly upstream of the *HindIII* site. The modified pAED4 vector was transformed into *E. coli* BL21(DE3) pLysS cells (Stratagene). The *E. coli* cells were cultured in Luria Bertani medium in the presence of chloramphenicol and ampicillin, and expression of the Trp-(His)$_6$-hBD4 fusion construct was induced by addition of isopropyl β-D-1-thiogalactopyranoside (final concentration 1 mM). After additional 4-5 hours of incubation, cells were harvested by centrifugation, re-suspended in the lysis buffer (10 mM TrisHCl, 50 mM MgCl$_2$, 20 μg/ml DNase I, 20 μg/ml RNase A, 75 μg/ml lysozyme, and the *Complete*™ protease inhibitors cocktail, Roche Diagnostics GmbH, pH 8) and lyzed by two passages through a French press. After centrifugation, the pellet containing inclusion bodies was isolated and washed using standard protocols [43]. After solubilizing inclusion bodies in a solution of 6 M GdnHCl, 100 mM KPi, and 10 mM Tris buffer (pH 8.0), the Trp-(His)$_6$-hBD4 fusion protein was isolated using Ni-NTA agarose affinity chromatography (Qiagen) followed by precipitation with isopropanol (85%, v/v). Subsequently, precipitant was dissolved in 70% (v/v) formic acid and the mature hBD4 peptide was released from the fusion protein by cyanogen bromide (CNBr) cleavage according to a published protocol [44]. Products of the cleavage reaction were then dried (Rotavapore, R124VP, Büchi, Switzerland), re-dissolved in a small volume of water (to extract remaining traces of CNBr) and dried again. The resulting brown oil was solubilized in solution containing 6 M GdnHCl, 100 mM DTT, and 0.1 M Tris buffer (pH 8.5), and subjected to preparative reversed-phase (RP)-HPLC (POROS 20 R2 resin, PerSeptive Biosystems). Combined fractions containing the reduced form of hBD4 were freeze-dried. Folding and oxidation were accomplished by stirring the solution of hBD4 (0.1 mg/ml) in 0.1 M Tris (pH 8.5), 0.5 mM EDTA, oxidized

Table 2. Diffraction data. Statistics for data collection and processing.

Data for crystal of unmodified (di-Met)5-hBD4*	
Diffraction source	Beamline 22-ID, SER-CAT, APS, ANL, IL, USA
Wavelength (Å)	1.000
Temperature (K)	100
Detector	Mar CCD300 (Mar Research)
Crystal-to-detector distance (mm)¥	300, 200
Rotation range per image (°)	1.5, 2.0
Total rotation range (°)	225, 180
Exposure time per image (s)	15, 2
Space group	P43212
a, c (Å)	41.70, 52.95
Mosaicity (°)	0.34
Resolution range (Å)	50.0–1.58 (1.61–1.58)
Total No. of reflections	116,154
No. of unique reflections	6,966
Completeness (%)	100. (100.)
Multiplicity	16.7 (11.7)
$<I/\sigma(I)>$	90.3 (3.8)
Rmerge†,#	0.052 (0.644)
Rr.i.m‡,#	0.014 (0.213)
Overall B factor from Wilson plot (Å²)	35.8
CC1/2&,#	0.984 (0.906)

Data for Br-derivative crystal of (di-Met)5-hBD4§			
X-ray energy relation to anomalous edge of Br	„peak"	„inflection"	„remote"
Wavelength (Å)	0.92001	0.92021	0.91674
Resolution (Å)	30–2.3	30–2.3	30–2.4
No. independent reflections	3949 (2314)	3937 (2307)	3461 (2039)
Completeness (%)	100 (100)	100 (100)	99.9 (99.9)
Rmerge	0.079 (0.093)	0.074 (0.080)	0.059 (0.071)
Redundancy	7.4 (12.5)	7.3 (12.4)	4.2 (7.0)
Unit cell parameters a, c (Å)		41.66, 52.46	

Values in parentheses are for the highest resolution shell. ¥Underlined values correspond to the lower resolution pass. †$R_{merge} = \Sigma(|(I - <I>)| / \Sigma(I)$. ‡Estimated $R_{r.i.m.} = R_{merge} \Sigma[N/(N-1)]^{1/2}$, where N is the data multiplicity. &$CC_{1/2} = \Sigma(x - <x>)(y - <y>) / [\Sigma(x - <x>)^2 \Sigma (y - <y>)^2]^{1/2}$. #For more extensive definitions of these indicators see http://shelx.uni-ac.gwdg.de/~athorn/pdf/thorn_cshl2014_quality_indicators.pdf and the references cited therein. §Values are given for merging with Friedel pairs separate (and in parentheses with Friedel pairs combined).

(1 mM) and reduced (0.1 mM) glutathione, and 0.5 mM protein disulfide isomerase (Sigma-Aldrich) for 2 days at 4°C. Progress of oxidation was monitored by mass spectroscopy. The oxidized hBD4 was isolated by semi-preparative reversed-phase chromatography using YMC-Pack ODS-AP column (YMC) and its identity and purity were confirmed by analytical RP-HPLC and mass spectroscopy. For some crystallization experiments, in a fraction of pure hBD4 preparation, all primary amino groups were dimethylated according to the protocol described earlier [45], resulting in the (diMet)5-hBD4 product. Isolation and purification of (di-Met)-hBD4 was conducted analogously as described above for hBD4.

CRYSTALLIZATION X-RAY DATA COLLECTION,
STRUCTURE SOLUTION AND REFINEMENT

The initial crystallization trials were performed at 293 K using the Phenix crystallization robot (Art Robbins Instruments) and a wide range of commercial crystallization screens. After attempts to crystallize unmodified hBD4 failed, subsequent experiments were conducted with (di-Met)5-hBD4. Sitting droplets were prepared by mixing equal volumes (0.2 µl) of protein and reservoir solutions. After preliminary crystallization conditions were established, final optimization was performed manually. Further details on crystallization of (di-Met)5-hBD4 are depicted in table 1. For derivatization, crystals of (di-Met)5-hBD4 were soaked for 30 sec. in the reservoir solution containing lithium bromide at 0.5 M concentration. X-ray diffraction data were collected at the Advanced Photon Source in Argonne National Laboratory, (Argonne, IL, USA). Single crystals were mounted in Litholoops (Molecular Dimensions) and frozen in liquid nitrogen prior to performing data collection conducted at 100 K. The experimental images processed with subsequent scaling of reflection intensities using the programs HKL2000 and HKL3000 (HKL Research Inc.) [46]. Details of the collection of experimental data and statistics from subsequent processing are presented in table 2. Initial phases for the (di-Met)5-hBD4 structure were calculated using multiple anomalous diffraction (MAD) approach utilizing the diffraction data for Br-derivative of hBD4 at three different wavelengths (see tab. 2). For nine heavy atom sites identified with the program SHELXD [47], the best values of correlation coefficient (CC) and Patterson figure of merit were 0.496 and 0.159, respectively. Phases were subsequently improved with a companion program SHELXE [47]. At this stage the correct space group, P4₃2₁2, could be established, as indicated by values of pseudo-CC, contrast, and connectivity equal to 0.61, 0.53, and 0.92, respectively. Comparable statistics for the enantiomorphic space group, P4₁2₁2, were 0.47, 0.32, and 0.86, respectively. The initial model of (di-Met)5-hBD4, automatically generated with the program ARP/wARP [48] and improved by the program MR Rosetta [49], described positions of 40 amino acid residues arranged in two polypeptide chains as well as several solvent molecules. The latter calculations utilized X-ray data collected for the crystal of non-derivatized (di-Met)5-hBD4 within the resolution range of 25–1.6 Å. The final values of crystallographic R-factor and free-R were 0.29 and 0.36, respectively. At this stage, refinement of the structure continued with the program Refmac ver. 5.5.0104 [50] assisted by visual inspection and manual corrections aided by the program Coot [51]. In the final stages, B factors were refined according to the anisotropic model, which upon completion described positions for 43 amino acid residues, 17 water atoms, three sulfate and one trifuoroacetate anion. The final values of crystallographic R-factor

Resolution range (Å)	15.00–1.60 (1.64–1.60)
Completeness (%)	100 (100)
σ cutoff	None
No. of reflections, working set	5916 (416)
No. of reflections, test set	645 (46)
Rcryst	0.234 (0.290)
Rfree	0.268 (0.347)
No. of non-H atoms	
Protein	363
Ion	21
Water	17
Total	401
R.m.s. deviations	
Bonds (Å)	0.020
Angles (°)	2.050
Average B-factors (Å²)	
Protein	49.9
Ion	55.6
Water	74.8
Ramachandran plot	
Favored regions (%)	95.1
Additionally allowed (%)	2.4
Outliers (%)	2.4, Thr32
PDB code	5ki9

Values in parentheses are for the highest resolution shell.

and free-R were 0.230 and 0.268. Additional statistics from the final refinement are shown in table 3.

SEDIMENTATION EQUILIBRIUM (SE) MEASUREMENTS

SE analysis was carried out at 308 K in the Optima XL-A analytical ultracentrifuge (Beckman-Coulter Instruments) equipped with a four-hole An-60 rotor. The methodology used by us was reviewed previously [52]. During experiments, all solutions were enclosed in cells with the 12-mm optical path length. Solutions of hBD4 at concentrations of 37, 50, and 70 µM were prepared in two different buffers, 0.1 M Na-acetate (pH 4.6) with 0.2 M Li_2SO_4 (buffer 1, mimicking the crystallization conditions), and 0.14 M NaCl, 0.027 KCl, 0.01 Na_2HPO_4, and 0.01 KH_2PO_4 (buffer 2, pH 7.4, mimicking physiological conditions). Buffer densities and partial specific volumes (v-bar) were calculated by using the program SEDNTERP (www.jphilo.mailway.com/download.htm). The molar extinction coefficient of hBD4, ε_{280} = 10,185 $cm^{-1}M^{-1}$, was calculated from UV absorbance scans of the samples used for analytical ultracentrifugation. The rotor speeds utilized for data collection were 28,000, 33,000, 38,000 and 43,000 rpm. Sedimentation equilibrium absorbance data at radial increments of 0.002 cm with five repeats, recorded at 280 nm, were collected at all rotor speeds. Data analysis was performed with the programs ULTRASCAN (Version 6.0, www.ultrascan.uths.csa.edu) and WINNONLIN (Version 1.06, Pharsight, Mountain View, CA). SE profiles of the hBD4 solutions were calculated for four different models of which the first assumed that the protein formed homo-dispersed specimens and remaining models approximated one of three eqilibria, monomer:dimer, monomer:trimer, or monomer:dimer:tetramer.

The goodness of fit for each of these models was measured by values of root-square-mean deviations between the experimental and calculated SE profiles by the values of reduced chi-square (for details see, http://www.analytical-ultracentrifugation.com).

CHEMOTAXIS ASSAY

The migration of CCR6-transfected human embryonic kidney (HEK293) cells was assessed with a 48-well micro-chemotaxis chamber technique as previously described [53]. Samples of hBD2 and hNP1, used as positive and negative references, were prepared as described elsewhere [30,54]. The incubation times were 5 hours. The HEK293 cells were suspended in RPMI 1640 culture medium (Thermo Fisher Sci.), supplemented with 1% of bovine serum (Thermo Fisher Sci.). The same medium was used as a solvent for all protein solutions. Chemotactic activity was measured as the optimal concentration of test compound at which the highest chemotactic index is obtained.

ANTI-BACTERIAL ACTIVITY ASSAY

The antibacterial assays were conducted with *E. coli* ATCC 25922 (American Type Culture Collection). Samples of hBD2 and hNP1 were also included for reference. The bacteria were grown to a mid-logarithmic phase in tryptic soy broth, then diluted to 1x10⁶ CFU/ml in 10 mM potassium phosphate, 1% tryptic soy broth, pH 7.4. 100 µl aliquots of cells suspensions were incubated in the presence of different concentrations of peptides for 3 hours at 310 K. Subsequently, cells were serially diluted with the same buffer, then plated on Luria Bertani Broth plates. Colonies were counted after 18 hours of incubation at 306 K. Microbicidal activity was expressed as the ratio of colonies counted to the number of colonies on a control plate. All experiments were completed at least three times, and the average values are reported here. The LD_{xx} is a concentration of protein at which xx% of viable cells are killed.

RESULTS AND DISCUSSION

Till now, hBD4 remained very poorly characterized and the 3-dimensional structure of this defensin was unknown. As we shall discuss below, in the case of recombinant preparations of defensins, detailed structural characterization is particularly important for proper interpretation of results obtained during the biological/functional studies of these proteins. hBD4 is a small protein (50 a.a.) characterized by a very high content of charged residues (18 a.a. or 36% in addition to the termini), resulting in a net charge of +6. The other three well-described human β-defensins, hBD1-3, in addition to their potent microbicidal properties, are chemotactic for cells expressing the functional form of the chemokine receptor, CCR6, which is also a natural target of chemokine MIP-3α (or CCL20). This property was not investigated before for hBD4. In this project, we aimed to prepare the functional recombinant hBD4, determine its crystal structure, characterize its chemotactic properties, and search for correlations between the structural features and biological functions of this protein.

Most of the protocols used to prepare samples of soluble, active hBD4 were described by us earlier, while working on related defensins [31,54]. However, in response to an in-

creasing number of reports describing simple protocols for a "high-yield" expression of active defensins in bacteria, we would like to make here a few specific comments. Due to their strong antimicrobial properties, active and soluble defensins are not expressed in bacteria at levels sufficient for many subsequent studies including structural biology. Alternative approaches include an expression of their inactive forms in bacteria, use of eukaryotic expression systems, or chemical synthesis. In the past we utilized all of these approaches with a conclusion that the first of these methods is by far the cheapest and least demanding methodologically. Therefore, in this project hBD4 was expressed as an insoluble fusion with the N-terminal extension by the trp ΔLE 1413 polypeptide [42]. The inclusion of this specific leader sequence assured that hybrid polypeptide was targeted to bacterial inclusion bodies, and was innocuous to the growth of bacterial culture. Keeping defensins insoluble is critical for successful expression since even misfolded or "linearized" variants of these proteins are potent antimicrobials when solubilized [55]. The leader sequence was chemically removed by the cyanogen bromide cleavage at the site of methionine residue, separating sequences encoding trp ΔLE 1413 polypeptide and hBD4. Such an approach is possible only when sequences of target proteins do not contain methionine residues, which is usually true only for small proteins. Although our protocol for generation of active hBD4 was developed by necessity rather than appeal, it has a few positive elements. The expression yields of insoluble defensin fusions are usually very high and the product can be readily purified to a high degree prior to the folding process. After folding and final purification, we were able to obtain samples of hBD4 at a scale of tens of milligrams. The purity and chemical composition was confirmed by gel electrophoresis, analytical RP-HPLC, and mass spectroscopy. It should be mentioned that folding of defensins, associated with formation of three disulfide bonds, leads sometimes to a mixture of variants with different topologies of Cys-Cys connections. Because the last two Cys residues in the sequences of human defensins are adjacent, a specific topology of three disulfide bonds cannot be unambiguously resolved by such traditional approaches as partial enzymatic digestion coupled with mass spectroscopy. Thus the structural methods provide the definitive tool for complete identification of defensin molecules. Additionally, lack of protons linked to oxidized thiol groups makes NMR spectroscopy less suitable for this purpose.
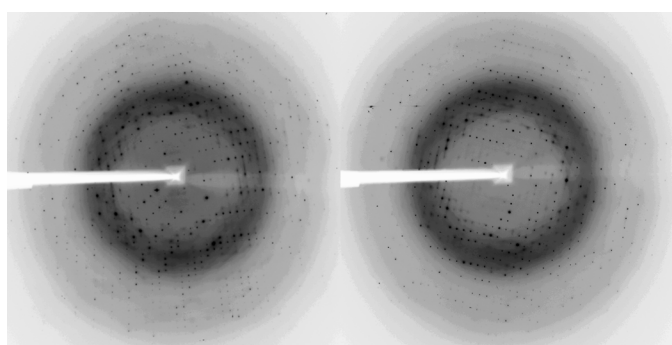
Figure 1. Diffraction images of hBD4 crystals, recorded using synchrotron X-radiation at the wavelength of 1 Å. Strong scattering component, especially at medium to low resolution, is evident for these crystals.

After multiple attempts to crystallize our preparation of hBD4 failed, we considered the possibilities of various modifications. At this stage, we excluded mutations due to possible structural effects and opted to increase hydrophobicity of the molecular surface by methylation of the primary amine groups; four Lys residues and the N-terminus in hBD4. It is necessary to stress that the methylated derivative of hBD4 was used only in the crystallographic experiments, while of all the biophysical and functional studies utilized the original unmodified preparation. Modified defensin, $(di\text{-}Met)_5$-hBD4, could be crystallized, and the resulting crystals diffracted X-rays to a resolution exceeding 1.6 Å. The typical diffraction image, recorded for $(di\text{-}Met)_5$-hBD4 crystals using a synchrotron source of X-rays is shown in figure 1. It is evident from this figure that many low- and medium-resolution reflections appear significantly diffused and some fraction of them are unusually intense. No crystal overexposure, no high mosaicity (here ~0.35°), nor a clear anisotropy of diffraction pattern are evident from images or from the data processing statistics. Also, no crystal twining of any type was detected from either diffraction pattern or distribution of reflections intensities. Consequently, we assumed that (i) diffraction from $(di\text{-}Met)_5$-hBD4 crystals contains large scattering component, most likely associated with either crystal or lattice defects, and (ii) unusually intense reflections result from a possible supersymmetry. Support for both claims is provided further in this section.

Despite the anticipated structural similarity to other human β-defensins, all attempts to solve the structure of hBD4 using the method of molecular replacement (MR) failed. Such an outcome was not completely unexpected and was observed by us earlier while working with mutated forms of hBD1 and hBD2. For such small proteins as defensins, any structural similarity of miniature cores of the model and target molecules is often completely countered by significant differences between equivalent flexible regions and/or side chains of non-conserved residues, rendering a template molecule unsuitable for MR searches. Subsequently, we collected X-ray data for crystals of Br-derivative. Using these data we were able to identify seven heavy atom sites using the program SHELXD [47]. Appropriate values of correlation coefficient (CC) and Patterson figure of merit were 0.496 and 0.159, respectively. Initial phases were improved with the program SHELXE [47]. This step also allowed a determination of the correct enantiomeric space group as $P4_32_12$ (values of pseudo-CC, contrast, and connectivity were 0.61, 0.53, and 0.92, respectively. Comparable statistics for the space group $P4_12_12$ were 0.47, 0.32, and 0.86, respectively). The initial structure of hBD4 was generated automatically with the program ARP/wARP [48]. The resulting model of hBD4 contained 40 amino acid residues (residues 2-41 in a monomer of defensin) and four water molecules. The crystallographic R-factor and Free-R values for this model, calculated for the resolution range 30.0–2.3 Å, were 0.27 and 0.35, respectively. Subsequently, the structure was subjected to an automatic rebuilding with the program MR Rosetta [49] against the X-ray data extended to the resolution of 1.60 Å, collected from a single crystal of unmodified $(di\text{-}Met)_5$-hBD4. This protocol resulted in the model describing 40 amino acid residues linked in one polypeptide chain,

however, values of R-factor and Free-R did not change significantly, 0.29 and 0.36, respectively. The subsequent steps included a manual rebuilding aided by the program Coot [51], interspersed by structural refinement using the program Refmac (ver. 5.5.0104) [50]. At final stages, the model for refinement of temperature displacement parameters was switched from isotropic to anisotropic. This operation was justified by a significant decrease of free-R value and an increase in figure of merit. During this process, the first 43 residues of (di-Met)$_5$-hBD4 could be modeled in the electron density. Additionally, three sulfate and one trifluoroacetate anions as well as 17 water molecules were added to the model and three Lys residues were replaced by dimethyl-Lys. At this stage, improvement of the structure was concluded. The final values of crystallographic R-factor and free-R are 0.230 and 0.268, respectively, and model is characterized by good sterochemistry. Except for a few side chains, all atoms of the model were well-described by a corresponding $2F_o$-F_c electron density, and no unexplained F_o-F_c electron density peaks outside the range –3.0 σ–3.0 σ were present.

The fact that the structure of hBD4 is in very good agreement with those known for other β-defensins and that it was fully derived from the experimental (unbiased) phases eliminates the possibility of an incorrect solution. Several observations, however, require some commentary. First, the agreement between the model and experimental intensities, represented by R values, is somewhat poorer than expected. Second, the number of modeled solvent molecules (17 waters) is lower than usually reported at the resolution of 1.6 Å. These two observations, together with detected earlier high scattering seen in the diffraction images, suggest to us a possibility of either random but significant defects in the crystal lattice or a highly dynamic character of structure/lattice. Both possibilities corroborate with the calculated value of mean B, equal to 51.2 Å^2. In addition, *a posteriori* calculations, in which the protein part of the final hBD4 model was used as a template in MR searches, well-packed solutions (without clashes) could be identified in both enantiomorphic space groups, P4$_3$2$_1$2 and P4$_1$2$_1$2. Whereas the likelihood of the P4$_3$2$_1$2 being a correct space group was much higher than for P4$_1$2$_1$2, a non-random agreement of either model with the experimental data (i.e. R value in P4$_1$2$_1$2 is less than 0.45) is rather uncommon. If not a result of twinning, it is most likely possible only for low molecular weight content of asymmetric unit, i.e. one copy of small protein. As mentioned earlier, no indication of twinning was detected, however, even when twinning was imposed during a refinement procedure, it did not lead to an improved agreement between the calculated and experimental data. Therefore, it seems that additional correlations, not described by standard crystallographic symmetries (i.e. supersymmetries) may exist in the crystal lattice of (di-Met)$_5$-hBD4. In conclusion, we suggest that further improvement of agreement between the current structure of (di-Met)$_5$-hBD4 and collected experimental data can be achieved by utilizing more elaborate modeling tools, accounting for scattering, which is beyond the goals of this project.

A single molecule of (di-Met)$_5$-hBD4, present in the asymmetric unit, shares the overall fold with other human β-defensins [15,30-32]. Its central part is arranged into a three-stranded antiparallel β-sheet and the structure of the whole molecule is stabilized by three disulfide bridges with a topology typical for β-defensins, Cys^I-Cys^V, Cys^{II}-Cys^{IV}, Cys^{III}-Cys^{VI}. These results confirm both the successful folding of hBD4 and a correct determination of its crystal structure. The N-terminal tail of this defensin (residues Glu1 through Tyr10) accommodates an extended conformation and forms the interface, comprising a series of H-bonds, with the equivalent region of a symmetry-related molecule in an antiparallel fashion. In the crystal, the C-terminus of (di-Met)$_5$-hBD4 is very flexible and its structure could not be elucidated. It is worth noting that this polypeptide chain hBD4 is the longest of five human β-defensins for which structural data are now available. Whereas the backbone of (di-Met)$_5$-hBD4 is well-defined in the electron density for the first 43 amino acid residues, conformations of a few terminal residues (Glu1 and Asp41-Glu42-Ser43) and of a short loop (Pro30-Asn31-Thr32) connecting strands β2 and β3, are more labile. Also, the poor quality of the electron density for several long side chains exposed on the molecule surface indicates their flexibility. Comparison of five human β-defensins is illustrated in figure 2, which clearly demonstrates structure conservation in the core regions of these proteins. The core regions of hBD4 and other β-defensins can be superimposed with r.m.s.d. values of 1.0 Å (hBD1, monomer A in PDB entry 1ijv), 1.4 Å (hBD2, monomer A in PDB entry 1fd3), 1.7 Å (hBD3, model 1 in PDB entry 1kj6), and 1.4 Å (hBD6, model 1 in PDB entry 2lwl). The fold conservation is quite impressive for proteins that share only six identical residues, although pairwise comparison indicates up to 25% a.a. sequence identity (hBD4 with hBD3). Two moderate structural differences between the cores of hBD4 and hBD1-3 are the result of single residue deletions in the former. Five of the six canonical Cys residues are present in the core regions, while the sixth cysteine is contributed in each defensin by the N-terminal section. The relative locations as well as stereochemistry of all three disulfide bonds are conserved for all β-defensins except hBD6. In the latter, stereochemistry of the disulfide bonds is very poorly defined, which is not uncommon in NMR structures. The structural similarity of hBD4 and other defensins ends abruptly, however, when the comparison extends beyond the core regions. Two very striking differences, clearly seen in figure 2, are a long C-terminus of hBD4 and the lack of a helical motif present in the other four β-defensins. When compared to hBD1-3, the chain of hBD4 past the last conserved Cys residue is longer by 10 to 13 amino acid residues. A structurally-defined section of the C-terminal tail in hBD4 (residues 39-43) forms a turn, however, the most terminal region of this protein does not accommodate a unique stable conformation. In turn, length of the C-terminal section in hBD6 is comparable to hBD4. Whereas a model of the complete hBD6 monomer is shown in figure 2, in the complete NMR-derived assembly of models (PDB: 2lwl), a polypeptide chain following the last Cys accommodates many divergent conformations, suggesting that similar to hBD4, this region is also disordered in hBD6.

The most striking structural difference between hBD4 and hBD1-3,6 is seen for the amino-terminal section. In previously reported structures of human β-defensins, this segment of several residues forms a well-defined helical motif, with the following chain lined against the molecular core.
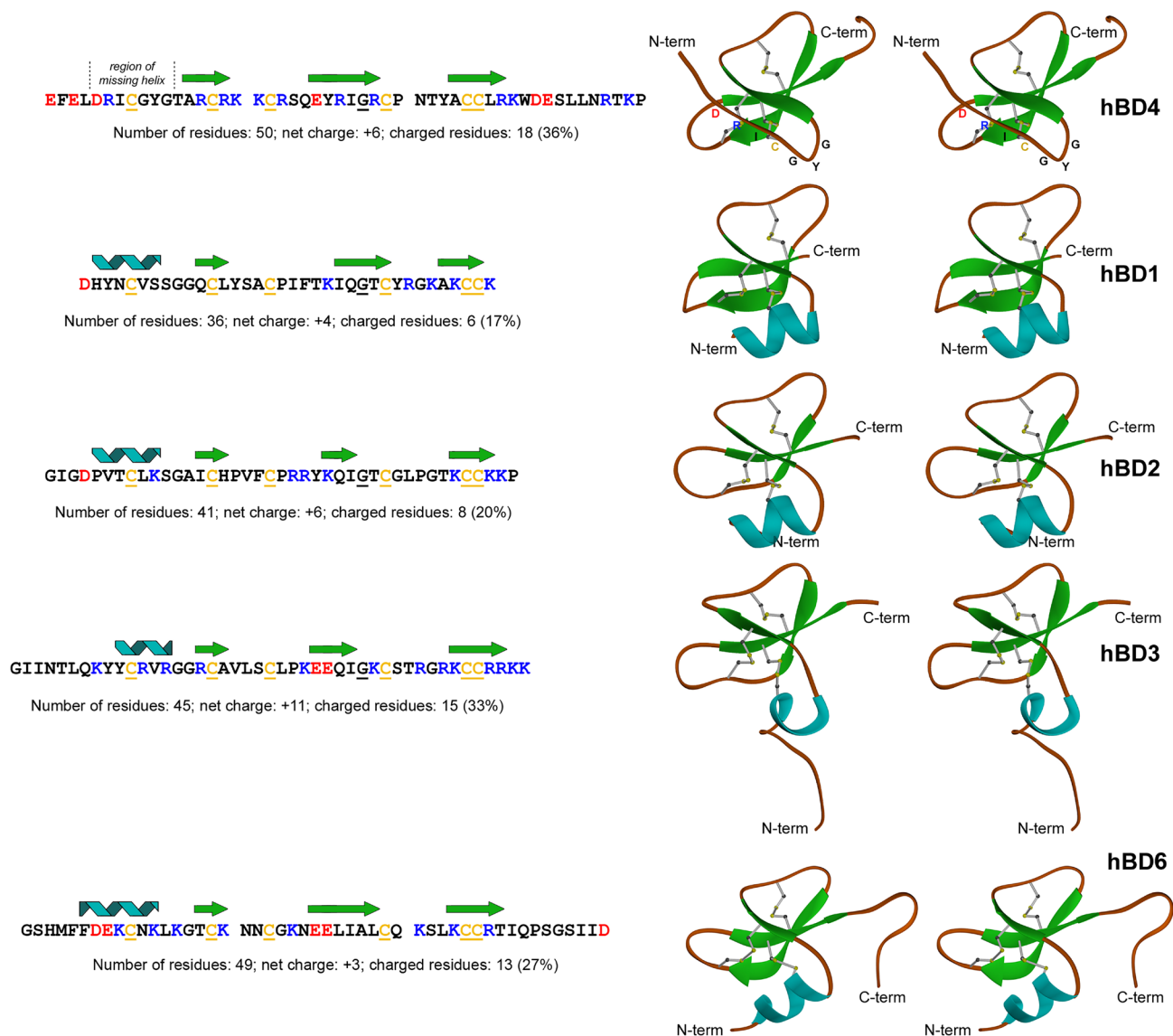
Figure 2. Amino acid sequences, aligned based on the conserved Cys residues and briefly annotated, are shown at the left. On the right, ribbon diagrams of uniformly oriented monomers are depicted in stereo.

In hBD4, however, no helical motif is present in the N-terminal region. Instead, the first nine residues in hBD4 adopt an extended conformation and transition towards the core via a turn-forming tripeptide (residues 10-12). The extended N-terminus of hBD4 projects away from the bulk of the molecule and is not stabilized by intramolecular interactions. Despite the dramatic topological differences between N-terminal sections of hBD4 and other hBDs, two structural details appear preserved. The side chain of the first canonical cysteine occupies nearly the same site in molecules of all four defensins, although its backbone in hBD4 is oriented in nearly opposite direction when compared to other hBDs due to different conformation, extended vs. helical. As a result, in the place of a hydrophobic side chain of the residue following the first cysteine, Val6 in hBD1 or Leu9 in hBD2, is in hBD4 occupied by a chemically similar side chain of the residue preceding Cys^I, Ile7. Analyses of hBD3 and hBD6 are more dubious as individual models within each of two

NMR assemblies describing these defensins are structurally quite variable in this region.

In contrast to α-defensins, no obvious dimerization was previously demonstrated for β-homologues. In a crystal of (di-Met)$_5$-hBD4, symmetry-related monomers form two types of dimers, detected during analysis utilizing the Web-based Pisa server (http://www.ebi.ac.uk/msd-srv/prot_int/cgi-bin/piserver, [56]). Molecular surfaces of the monomer and each of two dimers are 4083 Å^2, 6580 A^2, and 6980 Å^2, respectively. In the more compact dimer, associated with larger area of molecular surface buried upon dimerization, 792 Å^2/monomer (equivalent value for the second dimer is 595 Å^2), the primary interface is formed by the N-termini of hBD4 molecules. As seen in figure 3, in this dimer, a symmetric network of six main chain H-bonds connects two N-terminal sections into the anti-parallel β-sheet. The network includes Glu1(O), Glu3(N), and Glu3(O) atoms from one monomer interacting with Ile7′(N), Asp5′(O),
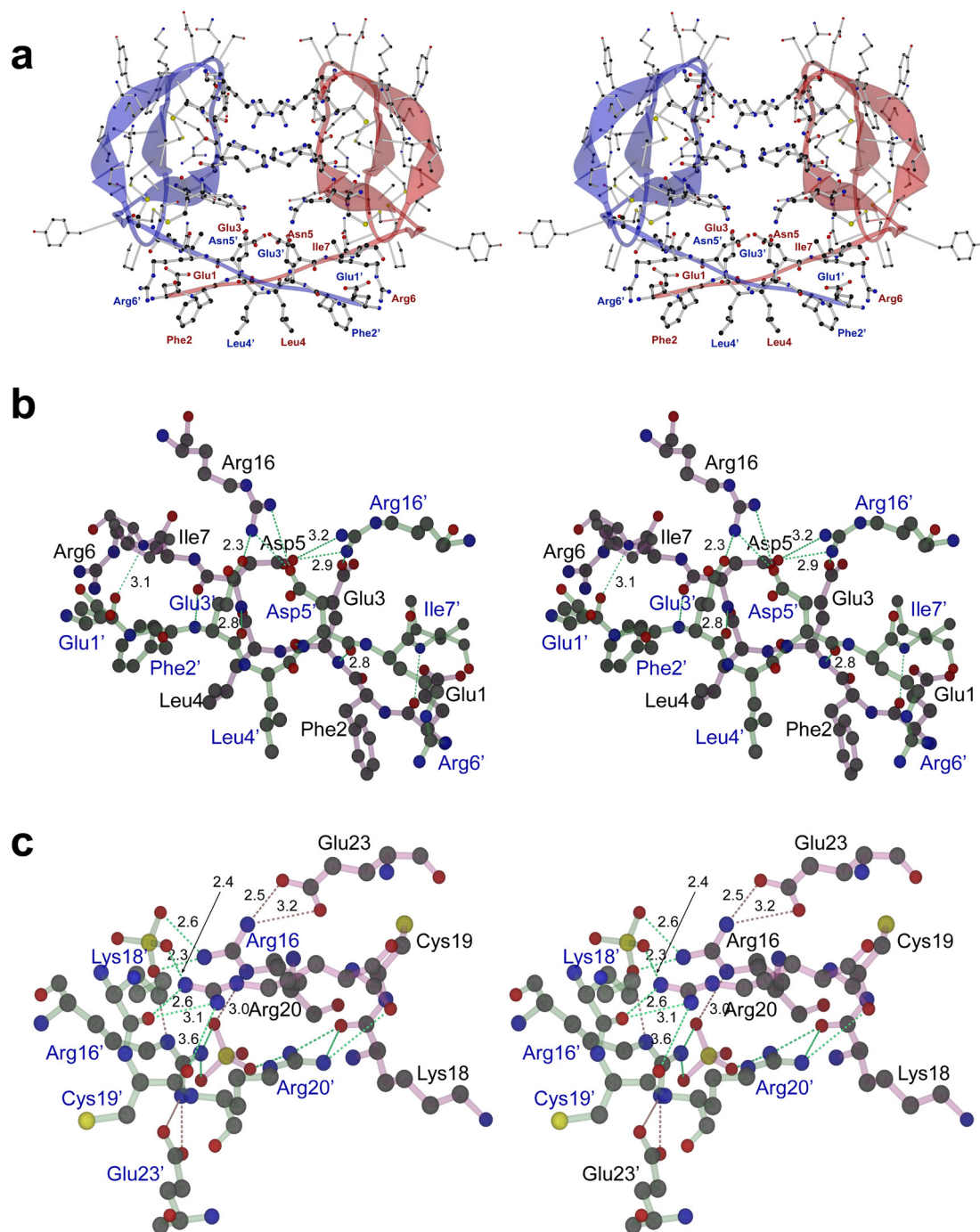
Figure 3. (A) Stereo view of the crystallographic hBD4 dimer. Monomers colored in blue and red, respectively, are depicted as semi-transparent ribbons with individual side-chains shown in ball-and-stick representation. Residues from the N-terminal sections of monomers are labeled. (B) The dimer-stabilizing interface, formed by the N-termini of two hBD4 monomers, colored red and green. A network of H-bonds is indicated by thin dotted lines. Since the interface is formed by crystallographic symmetry, distances are shown only for a half of H-bonds. (C) A region encompassing the pair of symmetry-related loops connecting strands β1 and β2 in each monomer located at the top of the dimer as shown in panel (A) of this figure. These loops contribute an additional set of dimer-stabilizing interactions, which are also marked here.

and Asp5′(N) from the second monomer, respectively. In addition to the network of six H-bonds, stabilization of the hBD4 dimer is provided by interactions between side chains of Phe2 and Leu4, which form a hydrophobic patch (Phe-Leu′-Leu-Phe′) on the surface of the dimer. In the crystal, this patch lines up against hydrophobic sites from symmetry-related molecules. Also the side chains of Glu3 and Asp5 form electrostatic interactions with the guanidinium group

of Arg14′ and the aromatic ring (NE1 atom) of Trp40′, contributed by the core and C-terminal regions from the second monomer. Other than the amino-termini of the hBD4 molecule, sections contribute to the dimer interface two additional H-bonds between the guanidinium group of Arg20 and the main chain oxygen atoms of Lys18′ and Lys19′. In summary, the structural studies of hBD4 resulted in two findings that are novel for human β-defensins; the extended confor-

Table 4. Summary of sedimentation equilibrium analysis for hBD4.

Buffer 1: 0.1 M Na-acetate and 0.2 M Li$_2$SO$_4$ (pH 4.6)					
Rotor speed [rpm]	Statistics and Association constant (K$_a$)[†]	Model of equilibrium used in calculations			
		Single species[‡]	2[M]↔[M]$_2$	3[M]↔[M]$_3$	4[M]↔2[M]$_2$↔[M]$_4$[§]
28,000	χ²	181.2	4.88	181.4	4.76
	r.m.s.d.	0.058-0.073	0.009-0.014	0.058-0.073	0.008-0.014
	K$_a$	n/a	6.31×10^8	1.01	1.20×10^{10}
33,000	χ²	120.3	6.80	NC[&]	5.12
	r.m.s.d.	0.024-0.068	0.010-0.016		0.008-0.014
	K$_a$	n/a	3.89×10^5		1.70×10^5
38,000	χ²	227.1	8.62	227.1	8.67
	r.m.s.d.	0.066-0.086	0.012-0.017	0.066-0.086	0.013-0.017
	K$_a$	n/a	1.26×10^6	1.00	1.26×10^6
43,000	χ²	206.8	7.28	NC[&]	7.52
	r.m.s.d.	0.061-0.082	0.012-0.014		0.012-0.015
	K$_a$	n/a	2.00×10^6		3.89×10^6
Buffer 2: 0.14 M NaCl, 0.027 KCl, 0.01 Na$_2$HPO$_4$, and 0.01 KH$_2$PO$_4$ (pH 7.4)					
Rotor speed [rpm]	Statistics and association constant (K$_a$)	Model of equilibrium used in calculations			
		Single species	2[M]↔[M]$_2$	3[M]↔[M]$_3$	4[M]↔2[M]$_2$↔[M]$_4$
28,000	χ²	48.9	2.58	48.9	2.57
	r.m.s.d.	0.017-0.056	0.004-0.011	0.017-0.056	0.007-0.009
	K$_a$	n/a	9.73×10^4	1.00	3.00×10^4

[†]Parameter χ² represents the global reduced chi-square (goodness of fit) whereas r.m.s.d. describes root-mean-square deviation between measured and modeled values of absorbance within a utilized radial range of the rotor. Both parameters are dimensionless. K$_a$ is the association constant, represented in M^{-1} and M^{-2} for dimerization and trimerization. [‡]K$_a$ is not applicable for the "single species model". [§]Two K$_a$ value represents only the dimerization component of the model (2[M]↔[M]$_2$). [&]Calculations for these models were not performed.

mation of the N-terminus, unique to hBD4 and, intimately related, the formation of dimers. In order to illuminate possible biological relevance of the new findings, we performed a series of biophysical and functional experiments. We used the sedimentation equilibrium (SE) analysis with aid of an analytical ultracentrifuge to evaluate the oligomerization state of hBD4 in solution. The experiments were conducted in two different buffers, the first approximating the crystallization conditions and the second mimicking the physiological conditions. All experiments were performed with three different protein concentrations, using four centrifugation speeds. While our major objective was to determine whether hBD4 forms a meaningful population of dimeric molecules, we tested the SE data against four different models. In addition to the monomer:dimer equilibrium, we tested scenarios assuming formation of trimers or tetramers of hBD4, and the model with hBD4 present in a mono-dispersed form. We completed a semi-global analysis for each centrifugation speed fitting a tested model against the combined data acquired for solution with three different protein concentrations. The representative results are shown in the table 4. In the series of experiments completed under conditions similar to those used for crystallization of hBD4, we found that the monomer:dimer equilibrium best describes the experimental data. For this model, the reduced global chi-square value (χ²) averages near 7.0 for different rotation speeds and residuals (discrepancies between experimental and calculated data) are quite small. The approximated value of the dimerization constant is between 0.4×10^6 and 630×10^6

M^{-1}, which corresponds to the dimer dissociation constant K$_d$ within the range between 1.6 nM and 2.5 µM, suggesting that at sub-milligram/ml concentrations most hBD4 dimerizes. In comparison, values of χ² for the mono-dispersed model and a monomer:trimer are in hundreds (120-230) with significantly higher r.m.s.d. values. The agreement between experimental and calculated data is also quite good for the model accounting for a formation of hBD4 tetramers. However, because no additional improvement of statistics for this model compared to a simple dimerization was found, we do not consider these results to support a formation of hBD4 tetramers in solution. Our results of SE analysis suggest a presence of dimeric hBD4 in the solution under conditions similar to those used for crystallization of this defensin. To evaluate a possible effect of pH and other components present in the medium (acetate, lithium or, sulfate ions), for the second round of the SE analysis we used solutions of hBD4 in a more physiologically relevant buffer (see tab. 4). Again, the experiments were conducted at four different centrifugation speeds and results of analyses were quite consistent with those obtained in the first series of measurements. To illustrate these results, we show in table 4 numerical values calculated for only one centrifugation speed. Cumulatively, the SE studies indicated that dimerization of hDB4 is not an artifact of crystallization, however, due to the lack of information on physiological concentrations of this β-defensin, the biological relevance of oligomerization remains unclear.

It is well documented that human β-defensins 1 through 3 interact with the chemokine receptor, CCR6 [12,30,31]. No such interaction was reported yet for either hBD4, hBD6, or for any α-defensin. Additionally, our earlier studies of the hBD1 mutants pointed towards the N-terminus of this defensin as a motif important for the CCR6-mediated activity [27]. In this work we subjected hBD4 to the chemotactic assay with the CCR6-transfected HEK293 cells. In parallel, the same experiments were conducted for hBD2 and human neutrophil peptide 1, hNP1 (α-defensin), two proteins for which chemotactic properties are well documented [31,57]. Here, hBD2 served as a positive control, while hNP1 was a negative control. The summary of results is shown in table 5 and figure 4A. Each of the three defensins was presented to HEK293 cells at concentrations spanning over the range of 1–10,000 ng/ml. Typically, a concentration of β-defensin inducing the maximum migratory effect (C$_{max}$) falls between 10 and 100 ng/ml, which is about 10 times higher than in case of chemokines [26]. Initially, the cell migration increases un-

Table 5. Summary of CCR6-mediated chemotactic activity of **hBD4, hBD2 and hNP1.**

| Molecule	Chemotactic Index[a]					Remarks[b]
Conc. [ng/ml]	1	10	100	1000	10,000	
hBD2(wt)	1.17 (0.15)	1.40 (0.14)	**1.84 (0.08)**	1.56 (0.11)	1.28 (0.18)	32
hBD4(wt)	1.07 (0.22)	1.06 (0.15)	1.08 (0.08)	1.12 (0.16)	1.20 (0.14)	14, inactive
hNP1(wt)	1.03 (0.14)	1.03 (0.15)	1.07 (0.16)	1.11 (0.14)	1.14 (0.09)	5, inactive

[a]Chemotactic Index (CI) represents the fold increase in the number of cell migration measured in the presence of test peptide over spontaneous cell migration in the presence of medium control. For each protein assayed, a value of highest CI is shown as bold-underlined numeral. Concentration of the protein, at which highest CI was observed, is referred as C_{max}. [b]Values shown in this column indicate numbers of independent experiments. Proteins characterized by the CI values near 1.0 for all tested concentrations are considered inactive. The "inactive" remark indicates an absence of the maximum in the "CI *vs.* concentration" profile within the concentration range tested.

til the concentration of a chemoattractant reaches C_{max}. Further increase of the concentration reduces chemotaxis due to effects associated with a saturation or desensitization of a targeted receptor. The absence of a maximum effect within the mentioned concentration range of chemotactic agent indicates either a lack of chemotaxis or lack of biologically-relevant chemotactic effect. Analysis of the data from table 5 clearly shows that hBD2 induces maximum migration of CCR6-transfected HEK293 cells at an approximate concentration of 100 ng/ml and, as expected, no chemotactic effect is observed for hNP1. Similar to the latter, CCR6-transfected cells seem to be non-responsive to different concentrations of hBD4. Therefore, hBD4 is the first documented human β-defensin that does not activate this receptor. By combining the results of structural studies and chemotaxis assay for hBD4 with our earlier research of the hBD1 mutants [55], we propose that the N-terminal region of β-defensins plays a central role in the CCR6-mediated chemotactic activity of human β-defensins.

Previously published reports described antimicrobial properties of hBD4 against several bacterial and yeast strains [33,35-37]. In all cases, preparations of hBD4 were either synthetic or recombinant, and were subjected to a fold-

ing protocol. Yet, the definite structural constitutions of these preparations were not demonstrated. Availability of pure, fully-characterized sample of recombinant hBD4 prompted us to subject this defensin to the bactericidal assay. Because our primary goals in this project were focused on structural and chemotactic properties of hBD4, we conducted the bactericidal assays using only one strain of bacteria, *E. coli* ATCC 25922. This strain of *E. coli* is a ubiquitous Gram-negative bacterium, best known for the ability to cause food-borne outbreaks [58]. As a reference, in these experiments, we also included well-defined and previously described preparations of hBD2 and hNP1. The results are illustrated in the figure 4B and values of LD_{xx}'s (representing concentration of an anti-microbial agent, necessary to kill xx% of treated bacteria) are shown in table 6. A high content of asymmetrically distributed basic residues, leading to an amphiphilicity of defensin molecules is broadly agreed to be a primary factor behind their microbicidal properties. The molecular surfaces of monomeric and dimeric hBD4, colored according to the electric potential, are shown in figure 5. The amphiphilic nature of this defensin is quite clear in case of the monomer where one face of the molecule is defined primarily by side chains of basic residues (top of panel A in fig. 5) while the opposite face is significantly less charged. This effect is less obvious for the dimer. In either case, however, an excess of basic residues is evident. The analysis of figure 4B and table 6 indicates that bactericidal properties of hBD4 against *E. coli* ATCC 25922 cells is comparable to that of hNP1 rather than to its closer homologue, hBD2. Although the molecules of both β-defensins, shown here, have equal net charge (+6) and the number of positively-charged side chains in hBD4 is significantly higher, 12, *vs.* seven in hBD2, it also contains six side chain carboxylates. In earlier studies of hBD1 mutants, we demonstrated
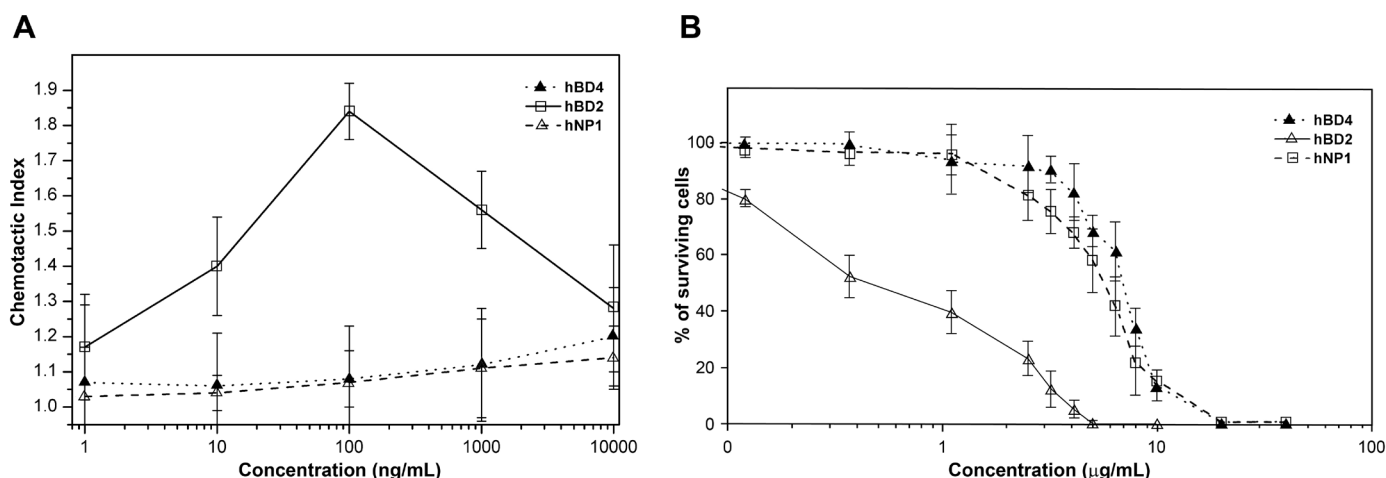
Figure 4. (A) Chemotaxis of CCR6-transfected HEK293 cells to hBD4, hBD2 and hNP1. Chemotactic activity was tested for different concentration of defensins as described in "Materials and Methods". The results are shown as profiles of CI *vs.* the defensin concentration. Each data point represents the average of five or more independent experiments, the values of mean errors are indicated by vertical bars. (B) Profiles of *E. coli* ATCC 25922 cells survival upon exposure to increasing concentrations of hBD4, hBD2 and hNP1 – the "kill curves" (also see the table 6).
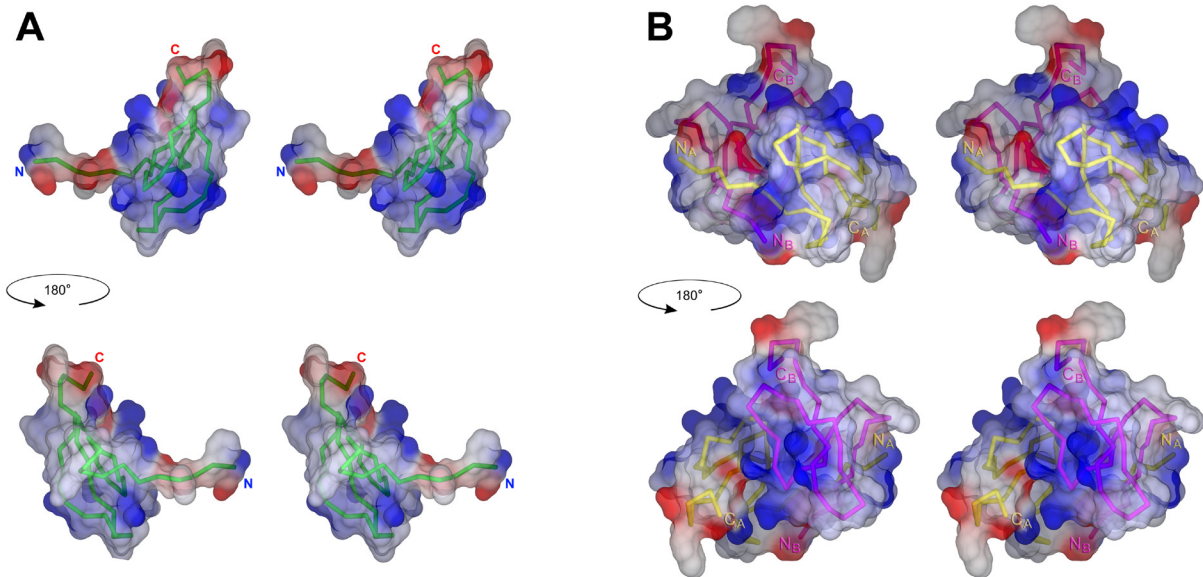
Figure 5. The ±5 kT/e electrostatic potential of hBD4, plotted on the solvent-accessible surface of monomer (panel A) and dimer (panel B). The stereo images were prepared with the programs PyMol [59] and POV-ray (http://www.povray.org/).

Table 6. The antibacterial activity of three human defensins tested against *E. coli* ATCC 25922 cells by the colony-counting method. LD_{xx} values are defined in the section "Materials and Methods". Values of the standard deviations (following the figures describing the LD_{xx} values) were obtained from three repetitions of each experiment. The concentrations of defensins used in these studies were in the ranges of 0–100 μg/ml.

Molecule	LD50 (μg/ml)	LD90 (μg/ml)	LD99 (μg/ml)
hBD2	0.5 ± 0.6	3.7 ± 0.5	4.9 ± 0.1
hBD4	7.0 ± 0.5	10.6 ± 0.8	12.0 ± 0.4
hNP1	5.5 ± 0.5	9.6 ± 0.8	41.0 ± 22.6

a strong attenuating effect of acidic residues on bactericidal properties against the same strain of *E. coli* [55]. It is possible that weaker bactericidal properties of hBD4 than hBD2 stem from similar foundations. The slope on the "kill curve" for hBD4 is visibly steeper than for hNP1 (see fig. 4B). Interestingly, the concentration range corresponding to this slope correlates with concentrations at which a significant fraction of hBD4 dimerizes, however, more extensive and accurate measurements are needed to ascertain this relationship.

While the current medical crisis associated with increasing resistance to antibiotics attracts very extensive studies focused on microbicidal properties of defensins, the information highlighting chemotactic properties of these proteins remains less explored. There is a qualitative difference between the nature of interactions associated with micobicidal and chemotactic activities as both are manifested at concentration ranges of defensins differing by a few orders of magnitude. Whereas antimicrobial activities stem from a high density of non-specific, electrostatic forces contributed by a population of positively-charged defensin molecules, a chemotactic effect results from a well-tuned interaction associating a single defensin molecule with a specific membrane-embedded receptor, here CCR6. Structural comparison of three human β-defensins, hBD1-3, activating CCR6-mediated pathways, reveals a common motif – the N-terminal α-helix contributing a disulfide-engaged

Cys residue – that is unique among vertebrate defensins. Alterations or removal of the helical region result in significant decrease of chemotactic properties. Since no other molecular feature is uniquely shared by these three proteins, we hypothesize that the N-terminal section of these proteins is directly involved in the activation of the receptor, CCR6, by human β-defensins. In summary, we believe that results presented in this report not only provide new data specific to hBD4 but also illuminate the molecular basis of CCR6-mediated chemotactic properties of the whole family of human β-defensins.

REFERENCES

1. Mallow EB, Harris A, Salzman N, Russell JP, DeBerardinis RJ, Ruchelli E, Bevins CL (1996) Human enteric defensins. Gene structure and developmental expression. J Biol Chem 271: 4038-4045

2. Selsted ME, Tang YQ, Morris WL, McGuire PA, Novotny MJ, Smith W, Henschen AH, Cullor JS (1993) Purification, primary structures, and antibacterial activities of beta-defensins, a new family of antimicrobial peptides from bovine neutrophils. J Biol Chem 268: 6641-6648

3. Lay FT, Anderson MA (2005) Defensins - components of the innate immune system in plants. Curr Protein Pept Sci 6: 85-101

4. Rodriguez de la Vega RC, Possani LD (2005) On the evolution of invertebrate defensins. Trends Genet 21: 330-332

5. Lehrer RI, Ganz T (2002) Defensins of vertebrate animals. Curr Opin Immunol 14: 96-102

6. Hoffmann JA, Hetru C (1992) Insect defensins: inducible antibacterial peptides. Immunol Today 13: 411-415

7. Schutte BC, Mitros JP, Bartlett JA, Walters JD, Jia HP, Welsh MJ, Casavant TL, McCray PB Jr (2002) Discovery of five conserved beta -defensin gene clusters using a computational search strategy. Proc Natl Acad Sci USA 99: 2129-2133

8. Pazgier M, Hoover DM, Yang D, Lu W, Lubkowski J (2006) Human beta-defensins. Cell Mol Life Sci 63: 1294-1313.

9. Zasloff M (2002) Antimicrobial peptides in health and disease. N Engl J Med 347: 1199-1200

10. Harder J, Schroder JM (2005) Antimicrobial peptides in human skin. Chem Immunol Allergy 86: 22-41

11. Yang D, Biragyn A, Hoover DM, Lubkowski J, Oppenheim JJ (2004) Multiple roles of antimicrobial defensins, cathelicidins, and eosino-

phil-derived neurotoxin in host defense. Annu Rev Immunol 22: 181-215

12. Yang D, Chertov O, Bykovskaia SN, Chen Q, Buffo MJ, Shogan J, Anderson M, Schröder JM, Wang JM, Howard OM, Oppenheim JJ (1999) Beta-defensins: linking innate and adaptive immunity through dendritic and T cell CCR6. Science 286: 525-528

13. Niyonsaba F, Ogawa H, Nagaoka I (2004) Human beta-defensin-2 functions as a chemotactic agent for tumour necrosis factor-alpha-treated human neutrophils. Immunology 111: 273-281

14. Rohrl J, Yang D, Oppenheim JJ, Hehlgans T (2010) Human beta-defensin 2 and 3 and their mouse orthologs induce chemotaxis through interaction with CCR2. J Immunol 184: 6688-6694

15. De Paula VS, Gomes NS, Lima LG, Miyamoto CA, Monteiro RQ, Almeida FC, Valente AP (2013) Structural basis for the interaction of human beta-defensin 6 and its putative chemokine receptor CCR2 and breast cancer microvesicles. J Mol Biol 425: 4479-4495

16. De Paula VS, Pomin VH, Valente, AP (2014) Unique properties of human beta-defensin 6 (hBD6) and glycosaminoglycan complex: sandwich-like dimerization and competition with the chemokine receptor 2 (CCR2) binding site. J Biol Chem 289: 22969-22979

17. Ganz T (2005) Defensins and other antimicrobial peptides: a historical perspective and an update. Comb Chem High Throughput Screen 8: 209-217

18. Sahl HG, Pag U, Bonness S, Wagner S, Antcheva N, Tossi A (2005) Mammalian defensins: structures and mechanism of antibiotic activity. J Leukoc Biol 77: 466-475

19. Chu H, Pazgier M, Jung G, Nuccio SP, Castillo PA, de Jong MF, Winter MG, Winter SE, Wehkamp J, Shen B, Salzman NH, Underwood MA, Tsolis RM, Young GM, Lu W, Lehrer RI, Bäumler AJ, Bevins CL (2012) Human alpha-defensin 6 promotes mucosal innate immunity through self-assembled peptide nanonets. Science 337: 477-481

20. Rausch JM, Wimley, WC (2001) A high-throughput screen for identifying transmembrane pore-forming peptides. Anal Biochem 293: 258-263

21. Fujii G, Selsted ME, Eisenberg, D (1993) Defensins promote fusion and lysis of negatively charged membranes. Protein Sci 2: 1301-1312

22. Lohner K, Latal A, Lehrer RI, Ganz T (1997) Differential scanning microcalorimetry indicates that human defensin, HNP-2, interacts specifically with biomembrane mimetic systems. Biochemistry 36: 1525-1531

23. Wu Z, Hoover DM, Yang D, Boulègue C, Santamaria F, Oppenheim JJ, Lubkowski J, Lu W (2003) Engineering disulfide bridges to dissect antimicrobial and chemotactic activities of human beta-defensin 3. Proc Natl Acad Sci USA 100: 8880-8885

24. Brogden KA (2005) Antimicrobial peptides: pore formers or metabolic inhibitors in bacteria? Nat Rev Microbiol 3: 238-250

25. Perez-Canadillas JM, Zaballos A, Gutiérrez J, Varona R, Roncal F, Albar JP, Márquez G, Bruix M (2001) NMR solution structure of murine CCL20/MIP-3alpha, a chemokine that specifically chemoattracts immature dendritic cells and lymphocytes through its highly specific interaction with the beta-chemokine receptor CCR6. J Biol Chem 276: 28372-28379

26. Hoover DM, Boulegue C, Yang D, Oppenheim JJ, Tucker K, Lu W, Lubkowski J (2002) The structure of human macrophage inflammatory protein-3alpha /CCL20. Linking antimicrobial and CC chemokine receptor-6-binding activities with human beta-defensins. J Biol Chem 277: 37647-37654

27. Pazgier M, Prahl A, Hoover DM, Lubkowski J (2007) Studies of the biological properties of human beta-defensin 1. J Biol Chem 282: 1819-1829

28. Tyrrell C, De Cecco M, Reynolds NL, Kilanowski F, Campopiano D, Barran P, Macmillan D, Dorin JR (2010) Isoleucine/leucine2 is essential for chemoattractant activity of beta-defensin Defb14 through chemokine receptor 6. Mol Immunol 47: 1378-13782

29. Taylor K, Clarke DJ, McCullough B, Chin W, Seo E, Yang D, Oppenheim J, Uhrin D, Govan JR, Campopiano DJ, MacMillan D, Barran P, Dorin JR (2008) Analysis and separation of residues important for the chemoattractant and antimicrobial activities of beta-defensin 3. J Biol Chem 283: 6631-6639

30. Hoover DM, Chertov O, Lubkowski J (2001) The structure of human beta-defensin-1: new insights into structural properties of beta-defensins. J Biol Chem 276: 39021-39026

31. Hoover DM, Rajashankar KR, Blumenthal R, Puri A, Oppenheim JJ, Chertov O, Lubkowski J (2000) The structure of human beta-defensin-2 shows evidence of higher order oligomerization. J Biol Chem 275: 32911-32918

32. Schibli DJ, Hunter HN, Aseyev V, Starner TD, Wiencek JM, McCray PB Jr, Tack BF, Vogel HJ (2002) The solution structures of the human beta-defensins lead to a better understanding of the potent bactericidal activity of HBD3 against *Staphylococcus aureus*. J Biol Chem 277: 8279-8289

33. Garcia JR, Krause A, Schulz S, Rodríguez-Jiménez FJ, Klüver E, Adermann K, Forssmann U, Frimpong-Boateng A, Bals R, Forssmann WG (2001) Human beta-defensin 4: a novel inducible peptide with a specific salt-sensitive spectrum of antimicrobial activity. FASEB J 15: 1819-1821

34. Fahlgren A, Hammarstrom S, Danielsson A, Hammarstrom ML (2004) beta-Defensin-3 and -4 in intestinal epithelial cells display increased mRNA expression in ulcerative colitis. Clin Exp Immunol 137: 379-385

35. Yanagi S, Ashitani J, Ishimoto H, Date Y, Mukae H, Chino N, Nakazato M (2005) Isolation of human beta-defensin-4 in lung tissue and its increase in lower respiratory tract infection. Respir Res 6: 130

36. Smiley AK, Gardner J, Klingenberg JM, Neely AN, Supp DM (2007) Expression of human beta defensin 4 in genetically modified keratinocytes enhances antimicrobial activity. J Burn Care Res 28: 127-132

37. Supp DM, Gardner J, Klingenberg JM, Neely AN (2009) Antibiotic resistance in clinical isolates of *Acinetobacter baumannii*, *Pseudomonas aeruginosa*, and *Staphylococcus aureus* does not impact sensitivity to human beta defensin 4. Burns 35: 949-955

38. Abe S, Miura K, Kinoshita A, Mishima H, Miura S, Yamasaki K, Hasegawa Y, Higashijima A, Jo O, Sasaki K, Yoshida A, Yoshiura K, Masuzaki H (2013) Copy number variation of the antimicrobial-gene, defensin beta 4, is associated with susceptibility to cervical cancer. J Hum Genet 58: 250-253

39. Sharma H, Mathew B, Nagaraj R (2015) Engineering of a linear inactive analog of human beta-defensin 4 to generate peptides with potent antimicrobial activity. J Pept Sci 21: 501-511

40. Sharma H, Nagaraj R (2015) Human beta-defensin 4 with non-native disulfide bridges exhibit antimicrobial activity. PLoS One 10: e0119525

41. Hoover DM, Lubkowski J (2002) DNAWorks: an automated method for designing oligonucleotides for PCR- based gene synthesis. Nucleic Acids Res 30: e43

42. Staley JP, Kim PS (1994) Formation of a native-like subdomain in a partially folded intermediate of bovine pancreatic trypsin inhibitor. Protein Sci 3: 1822-1832

43. Wingfield PT, Palmer I, Liang SM (2014) Folding and purification of insoluble (inclusion body) proteins from *Escherichia coli*. Curr Protoc Protein Sci 78: 6.5 .1-6.5.30

44. Gross E, Morell JL (1974) The reaction of cyanogen bromide with S-methylcysteine: fragmentation of the peptide 14-29 of bovine pancreatic ribonuclease A. Biochem Biophys Res Commun 59: 1145-1150

45. Rayment I (1997) Reductive alkylation of lysine residues to alter crystallization properties of proteins. Methods Enzymol 276: 171-179

46. Otwinowski Z, Minor W (1997) Processing of X-ray diffraction data collected in oscillation mode. Methods Enzymol 276: 307-326

47. Uson I, Sheldrick GM (1999) Advances in direct methods for protein crystallography. Curr Opin Struct Biol 9: 643-648

48. Lamzin VS, Wilson KS (1997) Automated refinement for protein crystallography. Methods Enzymol 277: 269-305

49. DiMaio F, Terwilliger TC, Read RJ, Wlodawer A, Oberdorfer G, Wagner U, Valkov E, Alon A, Fass D, Axelrod HL, Das D, Vorobiev SM, Iwaï H, Pokkuluri PR, Baker D (2011) Improved molecular replacement by density and energy guided protein structure optimization. Nature 473: 540-543

50. Murshudov GN, Skubák P, Lebedev AA, Pannu NS, Steiner RA, Nicholls RA, Winn MD, Long F, Vagin AA (2011) REFMAC5 for the re-

finement of macromolecular crystal structures. Acta Crystallogr D67: 355-367

51. Emsley P, Cowtan K (2004) Coot: model-building tools for molecular graphics. Acta Crystallogr D60: 2126-2132

52. Lebowitz J, Lewis MS, Schuck P (2002) Modern analytical ultracentrif-ugation in protein science: a tutorial review. Protein Sci 11: 2067-2079

53. Falk W, Leonard EJ (1980) Human monocyte chemotaxis: migrating cells are a subpopulation with multiple chemotaxin specificities on each cell. Infect Immun 29: 953-959

54. Pazgier M, Lubkowski J (2006) Expression and purification of recom-binant human alpha-defensins in *Escherichia coli*. Protein Expr Purif 49: 1-8

55. Pazgier M, Prahl A, Lubkowski J (2004) Structure/function analysis for human beta-defensin 1. Protein Sci 13(Suppl. 1): 84-84

56. Krissinel E, Henrick K (2007) Inference of macromolecular assemblies from crystalline state. J Mol Biol 372: 774-797

57. Pazgier M, Li X, Lu W, Lubkowski J (2007) Human defensins-struc-tures, chemical synthesis and recombinant production. Curr Pharm Des 13: 3096-3118

58. Minogue TD, Daligault HA, Davenport KW, Bishop-Lilly KA, Broomall SM, Bruce DC, Chain PS, Chertkov O, Coyne SR, Freitas T, Frey KG, Gibbons HS, Jaissle J, Redden CL, Rosenzweig CN, Xu Y, Johnson SL (2014) Complete genome assembly of *Escherichia coli* ATCC 25922, a serotype O6 reference strain. Genome Announc 2: e00969-14

59. DeLano WL (2002) The PyMOL Molecular Graphics System. San Car-los, CA: DeLano Scientific.

Ludzka β-defenzyna 4 – defenzyna bez "śruby"

Adam Prahl[1], Marzena Pazgier[2], Jerry Alexandratos[3], Jacek Lubkowski[3,✉]

[1]Wydział Chemii, Katedra Chemii Organicznej, Uniwersytet Gdański, ul. Wita Stwosza 63, 80-308 Gdańsk, Polska
[2]Division of Vaccine Research, Institute of Human Virology, University of Maryland School of Medicine, Baltimore, MD 21201, USA
[3]Macromolecular Crystallography Laboratory, Center for Cancer Research, National Cancer Institute, Frederick MD 21702, USA

✉e-mail: lubkowsj@mail.nih.gov

STRESZCZENIE

β-Defenzyny to niewielkie kationowe białka, charakteryzujące się dużą zawartością cysteiny. Uczestniczą one w wielu procesach dotyczących odporności organizmu, zarówno wrodzonej jak i nabytej. Wszystkie β-defenzyny posiadają silne właściwości antybiotyczne w stosunku do szerokiej grupy drobnoustrojów. Część ludzkich β-defenzyn (hBDs) posiada również właściwości chemotaktyczne w odniesieniu do ko-mórek produkujących specyficzne receptory chemokinaz. Dotychczas zidentyfikowano dwa receptory chemokinaz, CCR2 i CCR6, które są specyficznie aktywowane przez ludzkie β-defenzyny. W ludzkim genomie zidentyfikowano około 50 otwartych ramek odczytu posiadających motywy charakterystyczne dla β-defenzyn. Jednakże tylko trzy spośród tych defenzyn, hBD1-3, zostały szczegółowo scharakteryzowane, włącznie z dokładnym opisem ich struktur cząsteczkowych. Ponadto, skromne dane na temat biologicznych i antybakteryjnych właściwości dostępne są dla hBD4, oraz struktura cząsteczkowa w roztworze dla hBD6. Struktura krystaliczna hBD4, opisana w niniejszej pracy z rozdziel-czością 1.60 Å, ukazuje istotne różnice pomiędzy topologią cząsteczki tej defenzyny a strukturami hBDs opublikowanymi wcześniej. Badania krystalograficzne sugerują możliwość tworzenia dimerów hBD4, które są również obserwowane w roztworze w trakcie pomiarów sedymenta-cji przy użyciu ultrawirówki analitycznej. W przeciwieństwie to hBD1-3, hBD4 nie posiada właściwości chemotaktycznych na komórkach wy-twarzających CCR6. Molekularne podstawy tej różnicy mogą być związane bezpośrednio z nietypową konformacją N-końca cząsteczki hBD4. Testy antybakteryjne z użyciem komórek *E. coli* ATCC 25922 potwierdzają opublikowane wcześniej silne właściwości bakteriobójcze hBD4.